Quantum Electronics **49** (6) 604–611 (2019)

LASER SPECTROSCOPY https://doi.org/10.1070/QEL16859

Measurements of a fully resolved contour of the carbon dioxide absorption line in a band at $\lambda = 1.605$ μm in the atmospheric column using high-resolution heterodyne spectroradiometry

S.G. Zenevich, A.Yu. Klimchuk, V.M. Semenov, M.V. Spiridonov, A.V. Rodin

Abstract. **We consider the application of the heterodyne signal detection technique to measure the atmospheric transmission spectrum in the near-IR range, which makes it possible to measure for the first time the contour of a separate line of the vibrational–rotational CO_2 band on the solar observation path with a high spectral resolution of $\lambda/\delta\lambda = 10^8$. Together with other characteristics of the instrument, this enables us to measure the carbon dioxide content in the atmospheric column with high accuracy. The experimental setup and measurement technique are described. The existing facilities for measuring the content of greenhouse gases in the atmosphere are compared, demonstrating the possibility of using the near-IR heterodyne spectroradiometry to develop a useful and competitive instrument that can be used in building new networks of ground stations to monitor greenhouse gases.**

Keywords: *laser spectroscopy, heterodyne spectroscopy, infrared range, remote sensing, greenhouse gases.*

1. Introduction

The development of climate models and relevant practical techniques for assessment of the natural and anthropogenenous impact on the climate system require the use of increasingly accurate instruments to determine the chemical composition of the atmosphere. In particular, to assess the emission intensity of greenhouse gases (GHGs), such as CO_2, CH_4, N_2O, and NO, it is necessary to measure their content in the atmosphere with sub-percentage accuracy. Due to significant variations in the GHG content in the surface layer, measurements are carried out, as a rule, by means of remote sensing, either from a satellite's orbit, or using ground stations. Commonly, due to the relatively high abundance of carbon dioxide in the atmosphere (about 400 ppm), measurements are performed on the weak (unsaturated in the atmospheric column) overtone lines of vibrational–rotational bands in the near-IR range at $\lambda = 1.58$, 1.9 and 2.02 μm.

One of the most well-known systems for ground monitoring of the GHG content in the Earth atmosphere is the international Total Carbon Column Observing Network (TCCON) [1] established in the early 21st century to supplement and validate data obtained from the SCIAMACHY, GOSAT, and OCO/OCO-2 satellite missions. This organisation includes up to 30 monitoring stations located around the world. TCCON is a network of ground-based 125HR Fourier spectrometers (Bruker Optics GmbH), which allow measurements in a wide spectral range (3900–15500 cm^{-1}), and the travel of its movable arm reaching 0.45 m provides spectral resolution up to ~ 0.02 cm^{-1}. Despite the measurement regime stability and high restoration accuracy of the GHG column abundance in the atmosphere, reaching $\sim 0.25\%$ for carbon dioxide, monitoring stations based on this spectrometer have several drawbacks. These are a high cost, large size and mass of the instrument, as well as the need for infrastructure and qualified personnel. All this imposes significant restrictions on the mobility of TCCON stations and the coverage density of measurements around the globe. At the same time, the expansion of the network of ground measurements is necessary, especially at those places where satellite observations are not possible due to their orbital parameters.

These drawbacks have inspired the attention of interested scientific groups to the development of more compact systems that could serve as an alternative to the existing TCCON stations. Thus, a compact instrument based on an EM27 commercial Fourier spectrometer (Bruker Optics GmbH) has been developed at the Karlsruhe Institute of Technology (Germany) [2]. The instrument with a dimension of $35 \times 40 \times 27$ cm, weight of 25 kg, and spectral resolution of 0.5 cm^{-1} can retrieve the CO_2 column abundance with an accuracy of 0.08%. Low power supply requirements and the instrument's Sun tracking system [3] associated with the instrument ensure its high mobility, as well as the capability of conducting measurements on mobile platforms. The instrument developers created a project called the Collaborative Carbon Column Observing Network (COCCON) and reported successful tests of EM27 spectrometers in collaboration with TCCON, which lasted three and a half years [4].

A group of authors from Japan proposed a compact instrument for remote sensing of the atmosphere, based on two devices [5]: a diffraction spectrometer operating in the spectral ranges 1565–1585 nm and 1674–1682 nm, and a high-resolution fibre-optic Fabry–Perot interferometer that was used for measurements in the spectral range of 1570–1575 nm. The GHG column abundance in the atmospheric column was

S.G. Zenevich, A.Yu.Klimchuk, V.M.Semenov Moscow Institute of Physics and Technology (State University), Institutskii per. 9, 141701 Dolgoprudnyi, Moscow region, Russia; e-mail: zenevich09@mail.ru;
M.V. Spiridonov Moscow Institute of Physics and Technology (State University), Institutskii per. 9, 141701 Dolgoprudnyi, Moscow region, Russia; A.M. Prokhorov General Physics Institute, Russian Academy of Sciences, ul. Vavilova 38, 119991 Moscow, Russia;
A.V. Rodin Moscow Institute of Physics and Technology (State University), Institutskii per. 9, 141701 Dolgoprudnyi, Moscow region, Russia; Space Research Institute, Russian Academy of Sciences, Profsoyuznaya ul. 84/32, 117997 Moscow, Russia

Received 15 October 2018; revision received 25 November 2018
Kvantovaya Elektronika **49** (6) 604–611 (2019)
Translated by M.A. Monastyrskiy

measured using this complex jointly with one of the TCCON network stations. Kobayashi et al. [5] report that the statistical error in the retrieval of the integral content of carbon dioxide and methane does not exceed 0.2%.

Heterodyne spectroscopy is a method that provides the highest possible spectral resolution. Even though this principle of spectral analysis is not yet widely used in commercial instruments, there is a significant amount of works on the development of heterodyne spectroscopy methods in the mid-IR range using quantum-cascade lasers [6, 7]. In our work, we consider the use of the optical heterodyning method for measuring the atmosphere transmission spectra in the near-IR range in order to accurately determine the GHG content.

Thus, in 2014, groups of authors from the Laser Remote Sensing Laboratory at the Goddard Space Flight Center, NASA, published and patented the concept of a compact heterodyne mini-LHR spectrometer [8, 9] based on a tunable diode laser emitting at a wavelength of 1573.6 nm and using a system of optical fibre couplers to superimpose the wave fronts. The first results of atmospheric transmission spectrum measurements with a fully resolved contour of a separate line of the vibrational–rotational CO_2 band in the selected spectral range were presented. The measurements were conducted using an AERONET suntracker, which, in particular, served as an entrance stage of the solar radiation input system into the spectrometer [10]. Retrieval of the carbon dioxide content resulted in an expected statistical error of ~ 8 ppm, which is significantly worse than modern requirements for ground GHG measurements. Subsequently, the instrument's noise characteristics and measurement errors were optimised, and the methane content was measured with an expected error of 10 ppb [11, 12]. These studies mention the possibility of both retrieving the vertical GHG concentration profile and designing a global GHG monitoring network using heterodyne spectrometers based on the well-developed AERONET network (about 500 stations worldwide). In 2017, Wilson et al. [13] proposed a prototype of a near-IR heterodyne spectrometer for installation on a CubeSat 4U microsatellite, and announced that it was possible to measure not only the carbon dioxide and methane content, but also that of water vapour, as well as to retrieve vertical profiles of their mixing ratios. In all the examples above, the instrument's spectral resolution did not exceed 10^6, which was mainly due to the lack of a separate channel for stabilising the heterodyne, which is based on a tunable distributed-feedback diode laser.

Studies in the field of near-IR heterodyne spectroradiometry, which have been conducted at the Moscow Institute of Physics and Technology since 2011, are based on the principle of stabilising the heterodyne along the reference absorption line. Klimchuk et al. [14] described in detail and implemented the technique of heterodyne radiation detection in the near-IR range. The tunable diode laser radiation was used as a reference signal, while the radiation from a similar laser operating at injection currents below the threshold value was used as a broadband signal. Single-mode fibre couplers were used to superimpose the wave fronts of the studied incoherent radiation and the local oscillator radiation. Work [15] describes in detail a heterodyne spectrometer prototype for measuring the GHG content by direct solar radiation and presents the results of measuring the atmospheric transmission spectra and vertical methane concentration profiles with an expected error not exceeding 1%. However, the developed prototype of the instrument had a number of drawbacks which greatly complicated the work with the data obtained. First and foremost, this refers to nonlinear distortions of the intermediate frequency (IF) signal, introduced by an analogue squared detector.

This paper presents an improved prototype of the heterodyne spectrometer with a high spectral resolution ($\lambda/\delta\lambda = \nu/\delta\nu = 10^7 - 10^8$, where $\nu = 1.8692 \times 10^{14}$ Hz is the laser radiation frequency and $\delta\nu = 10$ MHz is the width of the instrument's point spread function) for field measurements and also a technique for measuring the CO_2 content in the atmosphere, the accuracy of which is comparable to that demonstrated by the existing GHG monitoring stations based on diffraction spectrometers and high-resolution Fourier-transform spectrometers.

2. Experimental setup and methodology of the experiment

The schematic of the experimental setup is shown in Fig. 1a. A distributed-feedback diode laser (DL) (NTT EL, Japan), mounted in a 14-pin butterfly-type housing with a built-in Peltier thermoelectric element and a thermistor, was used. The DL linewidth is 2 MHz. The laser has a single-mode fibre output with an FC/APC-type connector, the end-faces of which are bevelled to prevent spurious reflection of the signal in the optical path. The laser radiation wavelength is 1.605 μm (6230 cm^{-1}) with a maximum output power of about 14 mW. The DL operates in quasi-continuous mode at a pre-set thermoelement temperature of 321.6 K and is pumped by trapezoidal current pulses with a duration of 39.4 ms and a repetition rate of 20 Hz. The DL temperature is stabilised at a level of $\sim 10^{-4}$ K using a feedback channel, and a fine tuning of the laser radiation frequency is performed by changing the pump current. A change in the pump current amplitude within the range of 70–95 mA provides the DL radiation frequency tuning in the range of 6229.75–6230.55 cm^{-1}.

The instrument has two optical channels: an atmospheric or heterodyne channel with a photodetector PD1, and a reference channel with a photodetector PD2 (Fig. 1a). For recording optical signals, use is made of Hamamatsu G9801-22 (PD1) and G8370-82 (PD2) broadband InGaAs detectors. Laser radiation enters the optical channels through a fibre-optic system based on single-mode silica optical fibre (OF) with FC/APC-type connectors and single-mode fibre couplers (FCs). These FCs serve both for splitting and coupling the optical signals: FC1 splits laser radiation into two channels in a 10/90 ratio, so that 90% of laser radiation is diverted to the reference multipass cell, and FC2 mixes the heterodyne signal and solar radiation in a 5/95 ratio, so that 95% are accounted for solar radiation passing through the atmosphere. In a single-mode FC, the condition of superimposing wave fronts for optical signals is automatically satisfied, and the diffraction divergence at the OF end-face meets the condition of the antenna theorem [16], which makes it possible to use the OF for heterodyne detection without any loss of the useful signal.

The basis of the reference channel used to stabilise the DL radiation frequency is a multipass cell of the ICOS system [17], which measures overall output radiation coming from the off-axis high-Q resonator. A schematic of a cell developed by the authors of this work is presented in Fig. 1b. It contains the following key elements: two plano-concave mirrors M1 and M2, an input collimator (IC) with a fibre-optic FC/APC connector, an input plano-convex lens L1 with a filter of 30 mm diameter ($\Delta\lambda = 1600 - 1650$ nm), an integrating plano-convex lens L2 (diameter 25.4 mm, $f = 20$ mm), and a photodetector

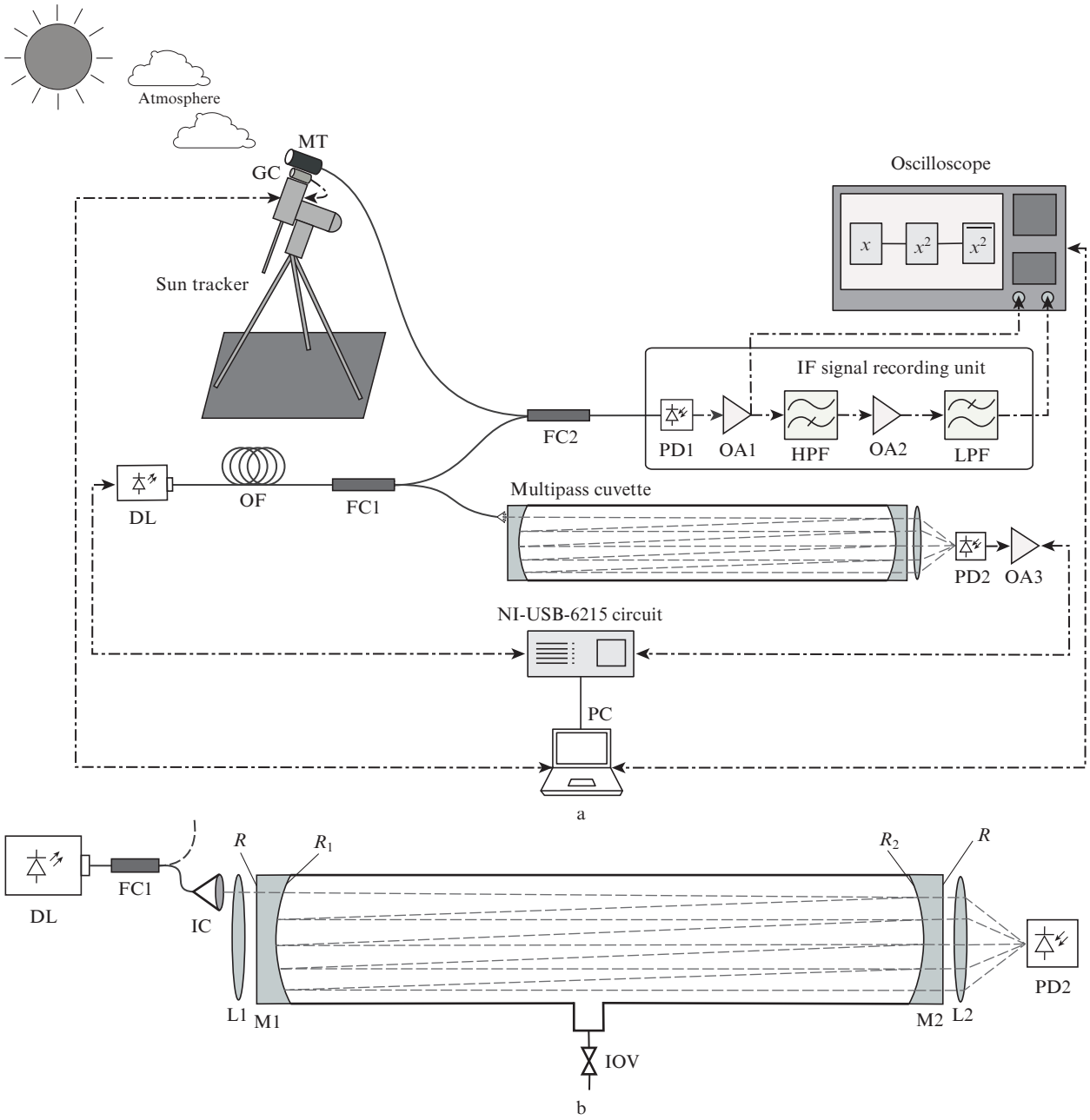

Figure 1. (a) Schematic of the experimental setup: (DL) diode laser; (OF) optical fibre; (FC) fibre couplers; (PD) photodetectors; (OA) operational amplifiers; (HPF) high pass filter; (LPF) low pass filter; (MT) microtelescope; (GC) guide camera; (PC) personal computer. (b) Schematic of the multipass cell: (M) and (L) mirrors and lenses; (IC) input collimator; (IOV) inlet/outlet valve; R is the reflection coefficient of the optical element surface.

PD2. The mirror substrates are made of quartz glass and have a diameter of 35 mm, thickness at the edges of 6.35 mm, and curvature radius of 500 mm. An antireflection coating with a reflection coefficient $R \sim 0.2\%$ is deposited on the flat side of each mirror. The concave side of mirror M1 has an 'ion deposition layer' with a reflection coefficient $R_1 \sim 99.98\%$, and the concave side of mirror M2 has an 'electron deposition layer' with a reflection coefficient $R_2 \sim 98\%$. The mirrors are mounted in an airtight aluminium alloy housing, so that the distance between their reflective surfaces constitutes 30 cm. The total cell volume is 212 cm^3. Due to the highly reflective mirrors, the cell performs the function of a resonator, in which, after multiple reflections, the low-intensity radiation transmitted through the mirror is focused by the integrating lens L2 onto photodetector PD2. The effective optical path length of the cell is ~30 m. An inlet/outlet valve (IOV) is placed on the lateral surface of the cell housing to connect the cell to the vacuum system. The cell was filled with pure CO_2 at a pressure of 150 mbar and, as mentioned above, was used for the DL temperature stabilisation and absolute calibration of the frequency scale. The choice of using the ICOS cell as an alternative to the multipass Herriot cell in the previous version of the spectrometer [15] was made for reasons of portability, convenience, and reliability of the system, as well as better stability to mechanical stress.

For relative calibration of the DL frequency, a Fabry–Perot etalon with a free dispersion range $D^* = 0.04933\ cm^{-1}$ was placed into the reference channel instead of the multipass cell.

The time sweep of the signal passing through the interferometer is shown in Fig. 2 (dashed curve). The spectral distance between adjacent signal maxima corresponds to the range of free dispersion of the D^* etalon. The recorded signal has been processed by a linearisation software module, the result of which is a tuning characteristic that collates the scales of the pump current and DL radiation frequency. This dependence made it possible to compensate for a nonlinearity of a change in the DL radiation frequency with a change in the pump current.

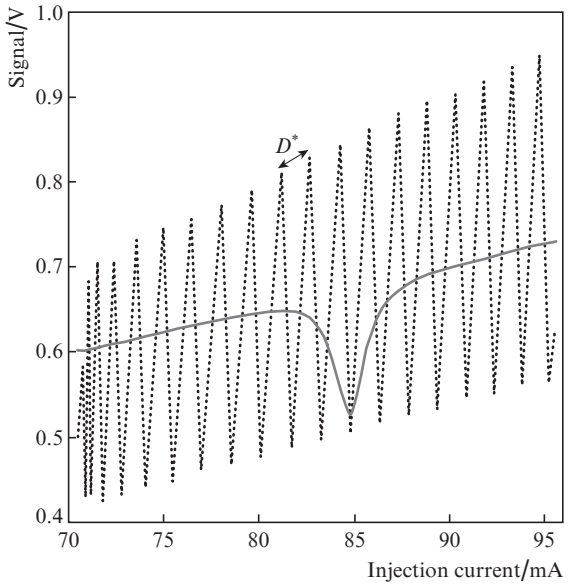

Figure 2. Radiation signal of the diode laser on PD2, passed through the ICOS multipass cell (grey curve) and Fabry–Perot interferometer (dotted curve).

The signal entering the heterodyne channel is recorded using photodetector PD1 and analysed by the IF signal recording unit, which represents a system consisting of a series of preamplifiers (PAs) and filters with an equivalent transimpedance gain of $r = 10$ MΩ and a bandwidth of $B = 0.2–10$ MHz. When using a narrow band for IF recording in the heterodyne regime, there is no need for an IF spectrum analyser, since, as described in work [14, 15], the signal spectral density in the low-frequency range is proportional to the noise dispersion. The IF recording unit has two outputs: the output from the first stage of the transimpedance amplifier (OA1), which converts the photocurrent into voltage, and the output from the bandpass filter (a combination of high-pass filters with a threshold of 0.2 MHz and low-pass filters with a threshold of 10 MHz), which extracts the analytical heterodyne signal having a form of white noise in the restricted frequency band. The signals from these outputs were fed to a two-channel RTO 1012 (Rohde & Schwarz) oscilloscope for initial processing. The signal from OA1 repeats the laser pulse shape and is only used to synchronise the oscilloscope with the measurement setup, while the signal after passing the bandpass filter is a useful signal containing information about the absorption line. The oscilloscope converts the incoming heterodyne signal in the 20 MHz band into digital form, squares and averages it. The signal converted in this way is transmitted from the oscilloscope to a PC. The oscilloscope is controlled in semi-automatic regime via an Ethernet channel using the LabView 12-based software.

Solar radiation transmitted through the atmosphere is fed into the OF using a specially developed automated Sun tracking system (tracker) based on a Sky-Watcher EQ6 PRO SynScan telescope mount and a QHY5-II guide camera (GC). The camera has the built-in servo drives which are controlled via the readings of the GC equipped with a short-focus (f = 3 mm) lens and a system of neutral filters attenuating the incident solar radiation intensity by 10^5 times. Filters are used to prevent damaging the CMOS matrix of the GC. In the tracking system, a microtelescope (MT) with a plano-convex lens (diameter 25.4 mm, f = 50 mm) and an FC/APC fibre connector holder on a ThorLabs uniaxial micromotor was installed. An optical signal chopper was also installed in the system for switching measurement regimes. The tracker was controlled by the MaxIm DL5 and StarCalc software. Although the described system has drawbacks, such as a large mass (40 kg) and the need for calibration when changing the measurement location, it can be aligned at the solar disk with an accuracy of 36″. The Sun tracking system has also undergone some improvements compared to the preceding spectrometer version described in [15]: it previously operated without a GC, only based on the built-in servo drives, which led to a decrease in the guidance accuracy and a drop in the solar radiation power recorded.

For controlling the laser and reference channel, a multifunction NI USB-6215 input/output controller is used, controlled using the LabView 12-based software developed by the authors. The controller represents a multifunctional electronic instrument that includes eight analogue-to-digital converters (ADCs) and two digital-to-analogue converters (DACs) with a bit depth of 16 bits and a sampling rate up to 250 kHz. In our case, the sampling rate in the measurement process was 5 kHz. One ADC channel and one DAC channel were used for the DL temperature stabilisation, one DAC channel – for controlling the DL injection current, and one ADC channel – for recording the signal from the PD2 reference channel. To reduce network interference, the installation is powered by a 12-volt battery. The instrument, with the exception of tracker and oscilloscope, is assembled in a compact case with a size of 60 × 50 × 23 cm and a mass of no more than 10 kg, and is controlled by an HP probook 6360b laptop with Windows 7 operating system using the abovementioned software.

Thus, laser radiation, pre-tuned to the desired spectral range by setting the DL temperature, propagates through the OF, and after the FC1, 90% of the DL radiation enters a multipass cell filled with pure carbon dioxide at low pressure. During the measurement cycle in the cell, the CO_2 absorption line (λ = 1.605 μm) shown in Fig. 2 (grey curve) is continuously recorded. By means of a specially developed algorithm, the line absorption peak position on the time scale is determined, and the pump current modulation cycle is corrected to ensure the absorption line to be located at the centre of the DL frequency tuning interval. Next, in accordance with the proportional-integral law, the DL radiation frequency tuning cycles are stabilised until the declared accuracy of 1 MHz is reached. In addition, the absorption peak position in the cell is used for absolute calibration of the DL radiation frequency.

After the passage of FC1, the DL radiation is coupled with solar radiation on the FC2 single-mode fibre coupler and fed to PD1. The heterodyne signal measurement technique in

the near-IR range is described in detail in [14]; here we only present its basic provisions. The photocurrent arising on the PD1 is proportional to the absorbed power of the incident optical signal, i.e. to the square of the electric field intensity. In our case, a mixed two-component signal is recorded. Then, the PD1 photocurrent is

$$i = D[|E_{LO}|^2 + (E_{LO}E_S^* + E_{LO}^*E_S) + |E_S|^2], \quad (1)$$

where D is the PD sensitivity; E_{LO} is the electric field intensity of the DL radiation; and E_S is the field intensity generated by a broadband radiation source (in our case, the Sun). The first and last terms in (1) correspond to the radiation intensities of the DL and broadband source. The second term in (1) is the useful IF signal:

$$E_{LO}E_S^* + E_{LO}^*E_S = 2\int_0^\infty E_{LO}(\omega)E_S(\omega) \times \exp[-\mathrm{i}(\omega_{LO} - \omega)]\mathrm{d}\omega + \text{c.c.} \quad (2)$$

In the narrow spectral range at low frequencies (0.2–10 MHz), the IF signal is noise with the spectral density $E_{LO}(\omega)E_S(\omega)$. The recorded standard deviation proportional to the IF spectral density has the form:

$$\sigma_{het} = r\sqrt{2Bi_{LO}\frac{\mathrm{d}i_S}{\mathrm{d}\omega}}, \quad (3)$$

where i_{LO}, i_S are the photocurrents due to DL and Sun radiations, respectively. This shows that, to record the atmospheric transmission spectrum, the useful IF heterodyne signal should be separated from the output PD1 signal and processed without hardware distortions. The function of IF signal separation is performed by the IF signal recording unit, and the processing function – by an oscilloscope. For greater clarity, it is appropriate to demonstrate the procedure for extraction and processing of a heterodyne signal using the schematic shown in Fig. 3. Figure 3a shows the shape of a single pulse of mixed radiation from the first output of the IF recording unit. After passing OA1, the signal intensity is expressed in voltage units and repeats the pulse shape of the DL injection current, i.e. has a trapezoidal shape, since the optical power is proportional to the DL pump current, and the photocurrent is proportional to the incident optical power. The noise depicted in this Figure is a heterodyne signal, the mean-square deviation of which is less than the pulse amplitude itself by several orders of magnitude (recall that Fig. 3 is a schematic). Figure 3b shows the signal from the second output of the IF recording unit after passage of HPF, OA2, and LPF. This is a filtered and amplified noise heterodyne signal containing information about

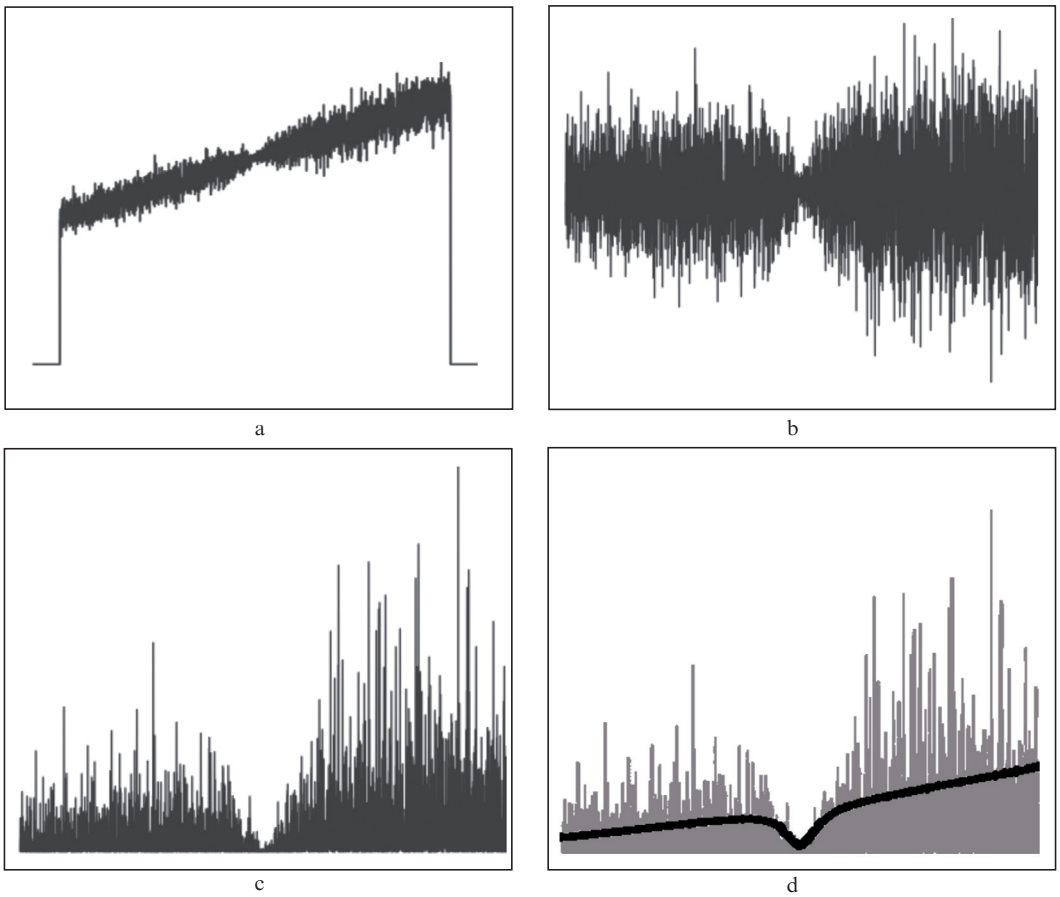

Figure 3. Schematic of the extraction and processing of an analytical noise heterodyne signal: (a) the signal from the first output of the IF signal recording unit (after OA1), the noise component shown against the main signal (the heterodyne signal); (b) the signal from the second output of the IF signal recording unit, i.e., the filtered heterodyne signal; (c) the signal after digitisation and squaring (the operation was performed with an oscilloscope); (d) the averaged noise dispersion (black curve) against a single measurement (grey signal).

the CO_2 absorption line in the atmosphere. Figure 3c demonstrates the signal shape after processing in the oscilloscope, i. e., after digitisation and squaring. Finally, the black curve in Fig. 3d shows the accumulated (averaged) signal, which represents the noise dispersion of the heterodyne signal on which the atmospheric absorption line is clearly visible. The accumulation procedure consists of two stages: 50 cycles of the IF signal measurements are averaged by an oscilloscope, and then the result is transmitted to a PC where 100 arrays are averaged. Thus, during one cycle, $N = 5000$ individual cycles of DL frequency modulation are averaged, which takes about 10 min with allowance for the 'dead' time needed to transfer data from the oscilloscope to PC. After processing the heterodyne signal, a slight slope of the dispersion curve becomes noticeable (Fig. 3d), which is explained by the dependence of the dispersion of the DL noise and the photocurrent on the DL pump current [14].

It should be noted that, in the previous version of the spectrometer [15], the signal processing procedure included analogue amplitude detection prior to its digitisation. This procedure may introduce nonlinearity at high DL pump currents, which results in additional uncertainty in the baseline position and complicates the retrieval of the integral GHG content in the atmosphere. The use of digital squared detection greatly facilitated the data processing procedure and enhanced the accuracy of quantitative measurements of the GHG content.

3. Measurement results

Atmospheric transmission spectra were measured on 2 August 2018 in the city of Dolgoprudnyi on the roof of a building located on the MIPT campus territory. The observation site coordinates were as follows: 55.929036° N, 37.521506° E, height above ground level ~ 50 m.

The experimental data in Fig. 4a represent the IF noise signal dispersion as a function of the DL pump current. The black curve corresponds to the dark signal when the chopper closes the solar radiation input into the microtelescope, and only the DL radiation enters the PD1. The grey curve corresponds to the heterodyne signal when the chopper opens the microtelescope and the mixed radiation enters the PD1. It can be seen from Fig. 4a that the heterodyne signal dispersion exceeds that of the dark signal. One may also notice a decrease in the signal noise dispersion in the range of DL injection currents corresponding to the frequency range of the CO_2 absorption line in the atmosphere. To obtain a heterodyne signal, it is necessary to subtract from the dispersion of the solar radiation signal the Schottky noise dispersion in the PD1 and the dispersion of intrinsic noise in the IF signal recording unit (those noises are contained in both signals) (see Fig. 4b, black curve) and divide the result by the estimated spectral continuum (baseline), i. e. the expected signal level in the absence of an absorber. To retrieve the baseline, a dark measurement signal was used, from which the Schottky noise level in the IF signal recording unit was subtracted. After that, the signal was approximated by a quadratic polynomial and normalised by an empirically selected coefficient of 0.131. The baseline thereby retrived is shown in Fig. 4b (grey curve). The resulting atmosphere transmission spectrum in the range of 6229.8–6230.6 cm^{-1} with a fully resolved contour of the isolated rotational line of the CO_2 vibrational–rotational spectrum ($\nu = 6230.227\ cm^{-1}$) is shown in Fig. 4c (black curve). Thus, the total data acquisition time for a single atmospheric

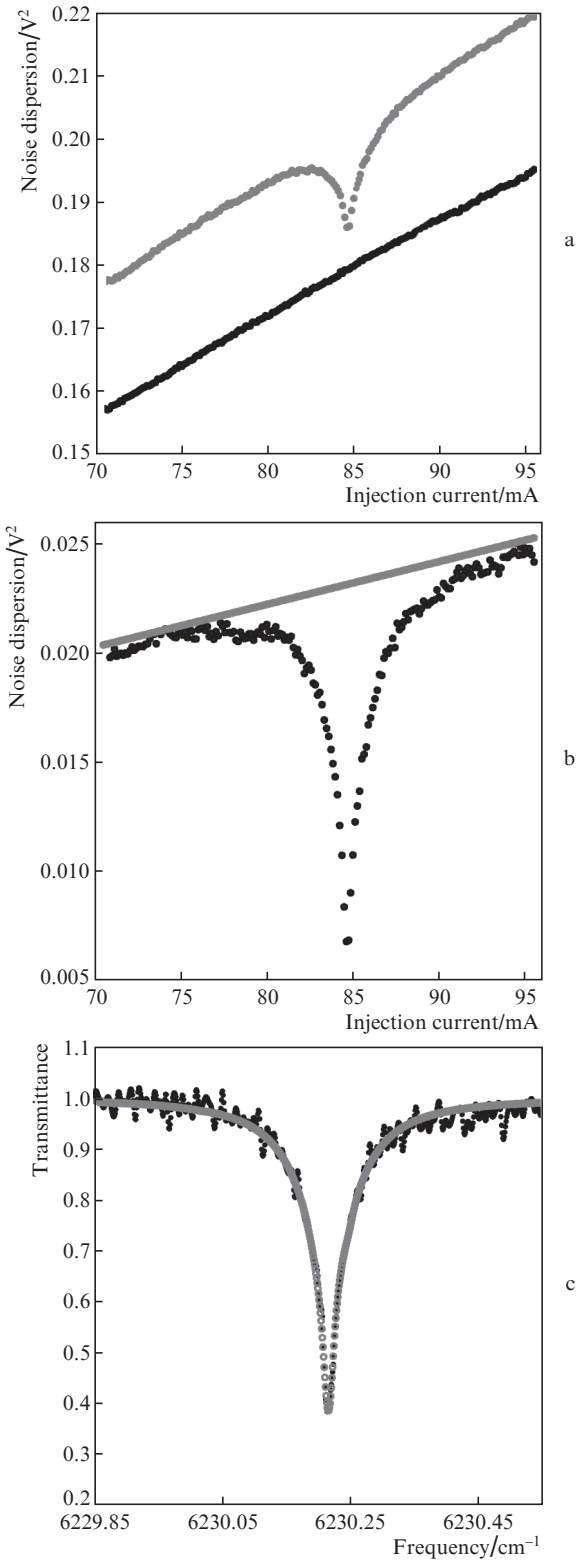

Figure 4. Experimental data and results of their processing: (a) the dispersion of the DL radiation noises as a function of the DL injection current when the PD1 recorded only the DL radiation (black line), and the solar noise dispersion as a function of the DL injection current when the PD1 recorded the mixed radiation (grey curve); (b) pure heterodyne signal (black curve) and a retrieved baseline, i. e. the signal level in the absence of an absorber (grey line); (c) the resulting transmission spectrum of the atmosphere with regard to relative and absolute calibrations (black curve), and the Voigt profile used to solve inverse problems (grey curve).

transmission spectrum at which the signal-to-noise ratio of ~100 is reached constitutes 20 min.

The obtained spectra were analysed by a detailed calculation of the radiation transfer in the atmosphere [18]. At the studied frequency, the intensity of direct solar radiation many times exceeds that of the scattered component; therefore, to analyse the spectrum, it suffices to use the Bouguer – Lambert – Beer law [18]:

$$I(\nu) = I_0 \exp(-\tau(\nu)), \quad (4)$$

where I_0 is the intensity beyond the Earth atmosphere; and ν is the frequency.

The optical density $\tau(\nu)$ was determined by the method of multilinear calculation (line-by-line). The spectral interval under investigation was selected as to ensure that only a single gas, namely CO_2, could be observed. The main contribution was made by a line centred at a frequency of 6230.22 cm^{-1}, and along with this line, the absorption lines at frequencies of 6230.25, 6230.02 and 6229.98 cm^{-1} were taken into account.

To compare the measured atmospheric transmission spectrum with the results of simulation and subsequent retrieval of the carbon dioxide concentration, it is necessary to make allowance for the vertical structure of the atmosphere. Heights up to 50 km from the surface were considered. The upper limit of the model atmosphere was chosen so that the contribution of the higher layers was less than 0.1% of the total absorption. The atmosphere was considered plane-parallel, horizontally homogeneous, and consisting of 100 layers adjacent to each other. It was also assumed that carbon dioxide was mixed uniformly in each model layer. The optical density of the layer of absorbing molecules at each frequency is a sum of the absorption cross sections $\sigma_{ij}(\nu)$ for j-th line, multiplied by the concentration ρ_i in each i-th layer and the thickness l_i of this layer:

$$\tau(\nu) = \sum_j \sum_i \sigma_{ij}(\nu)\rho_i l_i. \quad (5)$$

Spectral line parameters were taken from the HITRAN 2016 database [19]. The ERA-interim [20] and NCEP/NCAR [21] open reanalysis databases were used to determine the atmospheric model parameters (vertical profiles of temperature and pressure). In the calculations of the gas absorption cross section, both the Lorentzian and Doppler line broadening were considered, with the frequency dependence of the absorption cross section defined by the Voigt contour [18].

The issue of GHG concentration retrieval from the high-resolution spectra is beyond the scope of this work; however, we need to consider here the error budget, which enables the assessment of the technique possibilities. Since carbon dioxide in the atmosphere is well mixed, the average value $X_{\rho_{CO_2}}$ of its concentration in the atmospheric column is commonly sought. If the transmission spectrum $\tilde{\tau}(\nu)$ is measured experimentally, the problem of concentration retrieval is reduced to the problem of minimising a residual in the radiation transfer model:

$$\left| \tilde{\tau}(\nu) - \left(\sum_j \sum_i \sigma_{ij}(\nu) \right) X_{\rho_{CO_2}} \right| \to \min. \quad (6)$$

The retrieval accuracy is mainly determined by the system noises and instrument drifts, whereas the contribution of the atmospheric model uncertainties and of the spectral parameters of molecular absorption to the resulting error is negligible. Numerical experiments on fitting the model spectra to the measured ones have shown that the expected accuracy of determining the mean values of the CO_2 concentration is ~2 ppm. To assess the contribution of various sources of errors to the measurements, a statistical analysis was performed by varying different parameters (amplitudes of instrument noises, temperature profiles, baseline level, etc.) within their uncertainties and assessing the effect of these variations on the retrieved CO_2 concentration. The relative contribution of various sources of errors to the measurement results are shown in Table 1, with the resulting error estimated within the assumption of quadratic contribution of all its components.

Table 1.

Error source	Error magnitude (%)
Schottky noises	0.2
Drifts and instrument noises	0.5
Atmosphere model	0.1
Baseline	0.55

Apart from the atmospheric and spectral parameters described above, it is necessary to make allowance for the number of absorbing molecules on the observation path, determined by the Sun zenith angle α_{zen}. For the date and time of the experiment (02.08.18, 13:08), the results of which are shown in Fig. 4c, the zenith angle $\alpha_{zen} = 38.2°$. Thus, the experimentally measured optical density was calculated by the formula

$$\tilde{\tau}(\nu) = -\cos(\alpha_{zen})\ln(T(\nu)), \quad (7)$$

where T is the transmittance, after which the above-described algorithm (6) was applied, which resulted in the average concentration value $X_{\rho_{CO_2}} = 402.3 \pm 2.2$ ppm.

4. Conclusions

We have demonstrated the results of measurement of the atmospheric transmission spectra in the range of 6229.75–6230.55 cm^{-1} using a compact high-resolution heterodyne spectrometer operating in the near-IR range. The resulting spectra contain a fully resolved contour of a solitary rotational line of the vibrational–rotational absorption spectrum of atmospheric CO_2. Full contour resolution is possible due to the application of the technique of heterodyne radiation retrieval alongside with the use of a tunable diode laser with a linewidth of 2 MHz as well as a reference channel with an ICOS cell for DL frequency stabilisation at 1 MHz in the line vicinity. A signal-to-noise ratio of ~100 has been reached at an accumulation time of 10 min. A procedure for processing the atmospheric transmission spectrum and retrieval of the CO_2 integral concentration in the atmospheric column with an accuracy of 2.2 ppm is presented, which meets the requirements to modern ground networks for the validation of the GHG satellite monitoring data but is inferior to the characteristics of TCCON stations. Further steps towards the technique improvement will be to replace the oscilloscope with a digital signal processing scheme based on a programmable logic integrated circuit, to replace the cumbersome Sun tracking system with a tracker based on a mobile stabilised platform equipped with an automatic guidance algorithm, and to supplement the existing channel for measuring the CO_2 con-

tent with the channels for measuring the content and vertical concentration profiles of methane and water vapour in the absorption bands at $\lambda = 1.65$ and 1.38 μm, respectively.

Acknowledgements. This work has been supported by the Russian Science Foundation [Grant Nos 15-12-20040 (A.V. Rodin)] and the Russian Foundation for Basic Research [Grant No. 18-29-24204 (S.G. Zenevich, M.V. Spiridonov)].

References

1. Wunch D., Toon G.C., Blavier J.-F.L., et al. *Philos. Trans R. Soc. London, Ser. A*, **369**, 2087 (2011).
2. Gisi M., Hase F., Dohe S., Blumenstock T., Simon A., Keens A. *Atmos. Meas. Tech.*, **5**, 2969 (2012).
3. Gisi M., Hase F., Dohe S., Blumenstock T. *Atmos. Meas. Tech.*, **4**, 47 (2011).
4. Frey M., Sha M.K., Hase F., et al. https://www.atmos-meas-tech-discuss.net/amt-2018-146/.
5. Kobayashi N., Inoue G., Kawasaki M., et al. *Atmos. Meas. Tech.*, **3**, 1103 (2010).
6. Hoffmann A., Macleod N.A., Huebner M., Weidmann D. *Atmos. Meas. Tech.*, **9**, 5975 (2016).
7. Stangier T., Sonnabend G., Sornig M. *Remote Sens.*, **5**, 3397 (2013).
8. Wilson E., McLinden M., Miller J., Allan G., Ott L., Melroy H., Clarke G. *Appl. Phys. B.*, **114**, 385 (2014).
9. Clarke G.B., Wilson E.L., Miller J.H., Melroy H.R. *Meas. Sci. Technol.*, **25**, 055204 (2014).
10. Holben B.N., Tanré D., Smirnov A., et al. *J. Geoph. Res. C: Oceans*, **106**, 12067 (2001).
11. Melroy H.R., Wilson E.L., Clarke G.B., et al. *Appl. Phys. B*, **120**, 609 (2015).
12. Wilson E.L. https://www.osapublishing.org/ViewMedia.cfm?uri=CLEO_AT-2016-ATh3J.2&seq=0.
13. Wilson E.L., DiGregorio A.J., Riot V.J., et al. *Meas. Sci. Technol.*, **28**, 035902 (2017).
14. Klimchuk A.Yu., Nadezhdinskii A.I., Ponurovskii Y.Ya., Shapovalov Yu.P., Rodin A.V. *Quantum Electron.*, **42**, 244 (2012) [*Kvantovaya Elektron.*, **42**, 244 (2012)].
15. Rodin A., Klimchuk A., Nadezhdinskiy A., Churbanov D., Spiridonov M. *Opt. Express*, **22**, 13825 (2014).
16. Siegman A.E. *Appl. Opt.*, **5**, 1588 (1966).
17. Moyer E., Sayres D., Engel G., et al. *Appl. Phys. B*, **92**, 467 (2008).
18. Timofeev Yu.M., Vasil'ev A.V. *Theoretical Fundamentals of Atmospheric Optics* (Cambridge International Science Pub., 2008; St. Petersburg: Nauka, 2003).
19. Gordon I.E. et al. *J. Quant. Spectr. Radiat. Trans.*, **203**, 3 (2017).
20. Dee D.P., Uppala S.M., Simmons A.J., et al. *J. R. Met. Soc.*, **137**, 553 (2011).
21. Kalnay E., Kanamitsu M., Kistler R., et al. *Bull. Amer. Meteor. Soc.*, **77**, 437 (1996).